Available online at www.sciencedirect.com
ScienceDirect
Ceramics International 38 (2012) 919–927
CERAMICS INTERNATIONAL
www.elsevier.com/locate/ceramint

Improved thermal shock performance of Al_2O_3–C refractories due to nanoscaled additives

V. Roungos *, C.G. Aneziris

Department of Ceramic, Glass and Construction Materials, TU Bergakademie Freiberg, Agricolastraße 17, 09596 Freiberg, Germany

Received 30 May 2011; received in revised form 2 August 2011; accepted 4 August 2011
Available online 11 August 2011

Abstract

Carbon bonded alumina refractories with approximately 30 wt.-% residual carbon after coking are widely used as functional components such as submerged entry nozzles, monobloc stoppers and ladle shrouds in steel casting operations. Compositions with less residual carbon after coking based on nanoscaled magnesium aluminate spinel ($MgAl_2O_4$), alumina nanosheets (α-Al_2O_3) and carbon nanotubes (CNTs) either as single additives or combinations have been investigated according to their physical, mechanical and thermo-mechanical properties. The combination of nanoscaled powders based on carbon nanotubes and alumina nanosheets lead to superior thermal shock performance with approximately 30% less residual carbon in comparison to commercial available material compositions.

Keywords: B. Nanomaterials; D. Alumina; D. Graphite; E. Refractories

1. Introduction

Carbon bonded alumina refractories are widely used in steel casting operations. Basic representatives of this refractory product group are the so called functional components, like submerged entry nozzles, monobloc stoppers and ladle shrouds, which are used in the continuous casting sector of steel production. For the most effective productivity of the steel plant, these high duty refractories need to fulfil a number of demanding and partial controversial properties: high corrosion and erosion resistance, low wettability against steel- and slag-melts, high thermal shock resistance, as well as high mechanical strength and oxidation resistance at elevated temperatures. An optimization of the above properties and thus the refractory performance can be achieved by an appropriate adjustment of their microstructure.

According to the state of the art, the so called antioxidants are being commonly used as additives to the Al_2O_3–C refractories, in order to improve their poor oxidation resistance as well as for mechanical reinforcement. Usually fine metallic powders (Si, Al) in the range of up to 150 μm are used as antioxidants, as well as carbides (SiC, B_4C, Al_4SiC_4, $Al_8B_4C_7$) and boron containing oxides (fluxes) in the range of up to 100 μm [1–8]. The improvement of the oxidation resistance is being achieved with respect to the following mechanisms: the antioxidants react with the CO(g) of the surrounding atmosphere forming SiO(g) (in case of adding Si or SiC) and reducing CO(g) to C(s), thus suppressing oxidation loss of carbon [2]. The formed SiO(g) further reacts with CO(g) and deposits a thin protective layer of SiO_2(s) on the graphite surface, thus reducing the active sites [6]. Furthermore, these reactions are accompanied with a volume expansion, which can seal the pores of the refractory [1,2]. This effect is being utilised in the case of using boron containing compounds as antioxidants, whereby a glass phase formation is sealing the pores of the refractory [2,3,8]. In many cases, various antioxidants are being used together for further improvement of the refractories performance [4,8].

Materials in the nanometer scale are being used for the development of innovative products in numerous technological fields for more than twenty years and nowadays with a rapid growing tendency [9]. The use of nanoscaled materials in carbon bonded refractory products was introduced in 2003 by Tamura et al. [10] and Aneziris et al. [11]. The main reason for the rather late implementation of nanoscaled materials in carbon bonded refractories was their extremely high production cost as well as difficulties to distribute homogeneous the

* Corresponding author. Tel.: +49 3731 393861; fax: +49 3731 392419.
E-mail addresses: vasileios.roungos@ikgb.tu-freiberg.de, vasilis.rougos@gmail.com (V. Roungos).

0272-8842/$36.00
doi:10.1016/j.ceramint.2011.08.011

nanoscaled powders in the refractory matrix. However, it is nowadays well known that even minor amounts of additives can achieve significant performance improvements of the refractories [12–19]. Moreover, the technical advances in process engineering have enabled not only the constantly increasing production of new nanomaterials in an industrial scale, but also their production in a cost-effective way [18]. Thus, the introduction of nanoscaled materials in refractory products is being investigated by many researchers and refractory producers in the last few years [20–23].

In terms of this contribution a commercial available composition for carbon bonded alumina functional refractories (Reference I) was modified by reducing the carbon content approximately at 20 wt.-% and nanoscaled materials were added in order to achieve at least the same performance according to thermal shock resistance and hot modulus of rupture.

2. Materials and methods

The raw materials used for the preparation of the investigated Al_2O_3–C compositions were white fused alumina fine grade (99.70 wt.-% Al_2O_3, 0.16 wt.-% Na_2O) with a maximal grain size of 0.20 mm (Treibacher Schleifmittel, Austria), tabular alumina coarse grade (99.50 wt.-% Al_2O_3, max. 0.40 wt.-% Na_2O) with a maximal grain size of 0.60 mm (Almatis, Germany), fine natural graphite grade (99.5 wt.-% < 40 μm) with 96–97 wt.-% carbon content (Graphit Kropfmühl, Germany), coarse natural flake graphite (95.0 wt.-% > 71 μm) with 94–96 wt.-% carbon content (Graphit Kropfmühl, Germany), fine metallic silicon powder (Elkem, Norway) of high purity (99.5 wt.-% < 150 μm) and the nanoscaled materials as listed in Table 1. A novolac type phenolic resin in both liquid and powder form (Momentive Specialty Chemicals, Germany) was used as binder and hexamethylene tetramine (Momentive Specialty Chemicals, Germany) was contributing as curing agent.

The preparation of the investigated Al_2O_3–C compositions (Table 2) was made according to the standard commercial practice: all raw materials were mixed at room temperature in an Eirich intensive mixer, whereby the nanomaterial-powders were added in several steps right after the liquid binder was introduced in the mix. After mixing, bar shaped samples (25 mm × 25 mm × 150 mm) were uniaxial pressed at 100 MPa. The pressed samples were then cured at 180 °C and subsequently coked at 1.000 °C for 5 h under reducing conditions (in a retort filled with coke breeze). The open porosity, bulk density and pore size distribution of the coked samples were measured with the aid of a mercury porosimeter. The phase composition and the microstructure of the samples were evaluated via X-ray diffractometry (XRD) and scanning electron microscopy (SEM) supported by energy dispersive X-ray spectroscopy (EDS). The mechanical and thermo-mechanical properties of 10 bar samples in each case were determined according to EN 993-6 for cold modulus of rupture (CMOR) and EN 993-7 for hot modulus of rupture (HMOR). The HMOR was measured at 1.400 °C, with a previous holding time of 30 min at this temperature for all tested samples. The thermal shock resistance (with compressed air) was measured with respect to ENV 993-11. The residual $CMOR_{TS}$ was determined after five thermal shock cycles. The registered strength loss due to thermal shock gives a first estimation about the expected thermo-mechanical performance of the refractories during their application.

Table 1
Technical data of nanoscaled additives.

Nanoscaled raw materials	Producer	Abbreviation	Purity (wt.-%)	Average particle size (nm)	Specific surface area (m^2/g)
Spinel ($MgAl_2O_4$)	IBUtec (Germany)	S10	>99.0	10 ± 3	100 ± 5
Alumina sheets (α-Al_2O_3)	Sawyer (USA)	AS	95.0–99.8	10–250	9–40
Multi wall carbon nanotubes(C)	Bayer MaterialScience (Germany)	BT	>95.0	–	>200
	Timesnano (China)	TN	>95.0	–	>200

Table 2
Investigated Al_2O_3–C compositions.

Raw materials	Compositions (wt.-%)								
	Reference I	Reference II	S10	AS	TN	BT	S10–AS	S10–TN	TN–AS
Fused alumina	25.3	29.1				29.1			
Tabular alumina	33.7	38.9				38.9			
Fine graphite	14.5	10.0				10.0			
Coarse graphite	14.5	10.0				10.0			
Novolac liquid	2.0	2.0				2.0			
Novolac powder	4.0	4.0				4.0			
Metallic silicon	6.0	6.0				6.0			
Sum	**100.0**	**100.0**				**100.0**			
Spinel			0.1				0.1	0.1	
Alumina Sheets				0.1			0.1		0.1
Chinese CNTs					0.3			0.3	0.3
German CNTs						0.3			

3. Results and discussion

3.1. Addition of nanosized $MgAl_2O_4$, Al_2O_3 and CNTs

3.1.1. Influence on the physical properties

The composition of Reference I is related to a commercial available mix with approximately 30 wt.-% carbon. By modifying the Reference I composition in means of reducing only its graphite content to 20 wt.-% without adjusting further the grain size distribution a non optimum packing density is generated. In terms of the present work the grain size distribution of the oxide fillers has been kept the same for all compositions. This is pointed out in Fig. 1, which shows the open porosity of the coked samples versus their pore diameter. A shift towards larger pore sizes over the complete pore diameter range can be readily seen comparing the Reference I composition (29 wt.-% graphite) with the Reference II composition (20 wt.-% graphite), both without any nanoscaled additives (Table 2). The mean pore diameters of the Reference I and the Reference II compositions were 0.5 μm and 1.8 μm, respectively. However, the open porosity of the Reference II composition was with 18.6% only slightly higher than that of the Reference I composition (18.0%). As for the bulk densities, the Reference II composition had with 2.51 kg/m^3 a higher value than the Reference I composition, as expected, due to its lower graphite content.

The influence of the added nanomaterials on the physical properties of the coked samples can be directly observed by comparing the compositions S10, AS, TN and BT with the Reference II composition. A decrease of the pore sizes of all compositions over the upmost pore diameter range is evident, regardless of their total open porosity and bulk density values, pointed out in the median pore diameter values of Table 3. The decrease of the pore sizes is attributed to the microstructural evolution of the refractory compositions (in situ fibre/whisker structures formation), as well as the very high specific surface area of the added nanomaterials (Table 1).

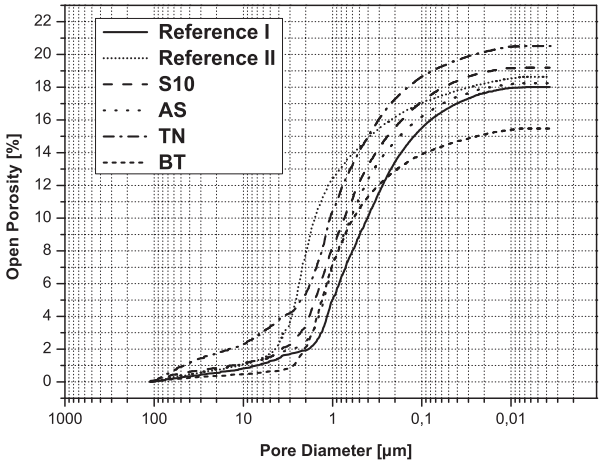

Fig. 1. Open porosity versus pore diameter of the coked samples with single nanoscaled additives.

Table 3
Physical properties of the coked Al_2O_3–C samples with single nanoscaled additives.

Compositions	Physical properties		
	Open porosity (%)	Bulk density (kg/m^3)	Median pore diameter d_{50} (μm)
Reference I	18.0	2.39	0.5
Reference II	18.6	2.51	1.8
S10	19.2	2.42	0.8
AS	18.2	2.50	0.7
TN	20.5	2.44	1.1
BT	15.5	2.55	0.9

3.1.2. Influence on the phase composition and the microstructure

The identification of crystallographic phases related to the addition of nanoscaled materials is not detectable with the aid of XRD-analysis, due to the extremely low content of the added nanomaterials. An associated shortcoming is the low degree of crystallinity of some phases, especially in cases of in situ formations of fibrous and/or whisker structures during the coking process at low temperatures like 1.000 °C, which is the case also of the present work [24]. However, this low coking temperature was deliberately chosen, since it is close to the industrial coking temperature in the range of 800 °C up to 1.000 °C. The above difficulties were revealed during the XRD-analyses, whereby only the major phases of corundum, graphite, β-alumina ($NaAl_{11}O_{17}$) and silicon could be identified.

The SEM micrographs of the two compositions without any nanoscaled additives (Reference I and Reference II) are shown in Fig. 2. The Reference I composition with graphite and silicon contents of 29 wt.-% and 6 wt.-% respectively, exhibited an in situ silicon-rich whiskers formation (Fig. 2a and b), as it was verified by the EDS analysis. The growth of the whiskers occurred at the pores of the refractory (Fig. 2a) during the coking process, with the growing mechanism being determined by a vapour–solid (VS) or a vapour–liquid–solid (VLS) reaction process, as it is known from the literature [25–29]. As for their morphology, the whiskers had a diameter of 50–100 nm and a length of up to several μm.

The reduction of the graphite content from 29 wt.-% to 20 wt.-% led to a highly differentiated microstructure of the Reference II composition. The absence of the in situ formation of whiskers (Fig. 2c and d) has a significant influence on the physical, mechanical and thermo-mechanical properties of the refractory, as it is presented in the next section of this study. It is known from the literature that the in situ formation of SiC fibres/whiskers in Al_2O_3–C refractories is depending on many parameters like coking temperature, concentration of the involved species (i.e. the chemical composition), partial pressure of CO(g) and porous microstructure. Many authors have reported in situ SiC-whisker formation at different coking temperatures, treating atmospheres and the content of the added silicon [5,30–32].

The microstructural evolution of the Al_2O_3–C refractories with nanomaterial additions – based on the Reference II composition – is shown in Fig. 3. The main characteristic was

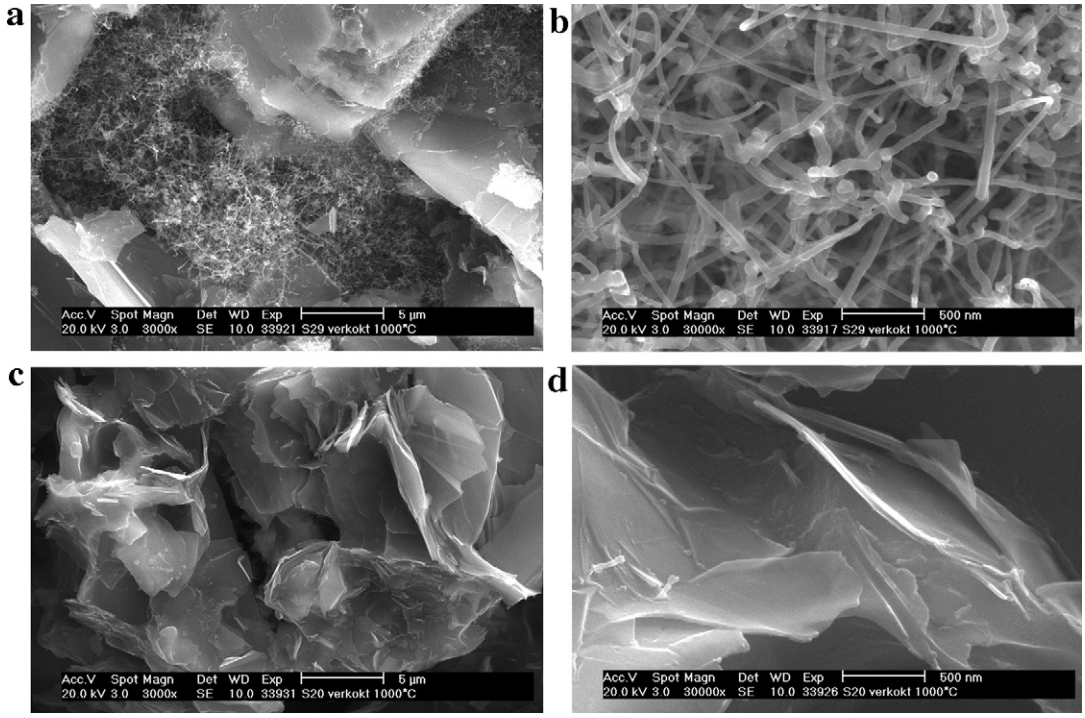

Fig. 2. SEM micrographs of fracture surfaces of Reference I and Reference II compositions: (a) Reference I, magnification: 3000×; (b) Reference I, magnification: 30,000×; (c) Reference II, magnification: 3000×; (d) Reference II, magnification: 30,000×.

the re-emerging of the silicon-rich whiskers in compositions S10, AS and TN (Fig. 3a–f), as it was confirmed by the EDS analysis. With the introduction of nanoscaled additives smaller pores are generated (Fig. 1) and subsequently the partial pressure and the concentration of the involved gaseous species are changed. Certainly, this has to be investigated in the future. Only composition BT exhibited no such microstructural development (Fig. 3g and h). This unexpected occurrence needs clarification and thus further investigation, taking into consideration the very high specific surface area of this nanoscaled material (Table 1). A possible explanation could be the granulated form of these CNTs as raw material [33]. Furthermore the additives for the granulation process of the CNTs could also be responsible that no whiskers were in situ formed.

3.1.3. Influence on the mechanical and thermo-mechanical properties

The microstructural differentiation of the Reference II composition compared to the Reference I composition had a direct impact on its mechanical properties, as it is pointed out in Fig. 4, in which the cold modulus of rupture (CMOR, left *Y*-axis), the open porosity (right *Y*-axis) and the average pore diameters (*X*-axis) of the coked samples are presented. The CMOR of the Reference II composition was with 12.6 MPa much lower than that of the Reference I composition (15.9 MPa), mainly due to the absence of the in situ whisker phase formation, presumably due to the higher pore diameters over the whole pore diameter range (Fig. 1). The addition of nanomaterials led to an increase of the mechanical strength of all compositions. Not only the in situ phase formation played hereby an important role (compositions AS, TN and S10) but also the morphology of the in situ structures formed, which is in turn related to the pore size distribution of the coked samples, as shown in Figs. 1 and 4. On the contrary, the total open porosity did not influence the mechanical strength of the coked samples, which is evident comparing the Reference II with the BT composition in Fig. 4.

The hot modulus of rupture (HMOR) of the coked samples was on the same level as their CMOR (Fig. 5), since the HMOR is mostly attributed to the advantageous hot strength of graphite. Compositions AS and particularly BT presented an increase in their HMOR values (16.0 MPa and 15.9 MPa respectively). The significant increase of the HMOR value of composition BT is attributed to the in situ whisker formation, which is evident for Al_2O_3–C refractories with silicon additives at 1.400 °C. On the contrary, the reduction of the HMOR of composition TN needs clarification, and thus further investigation.

As for the thermo-mechanical behaviour of the coked samples, expressed by the residual $CMOR_{TS}$ after 5 thermal shock cycles, all compositions exhibited lower strength losses compared to the Reference I composition (28.3%), as shown in Fig. 6. The lower strength loss of the Reference II composition (20.6%) is attributed to the higher pore sizes over the entire pore diameter range (Fig. 1) and the low CMOR value (with 12.6 MPa over 20% lower CMOR value than the Reference I composition). Higher CMOR values – like in the Reference I, AS and TN compositions – led to higher strength losses. Composition AS presented similar CMOR and HMOR values with the Reference I composition and exhibited a lower strength loss after thermal shock treatment, although having significantly lower carbon content (Fig. 6). It is obvious that a combination of porous structure and microstructural phase evolution during the coking process decisively contribute to the

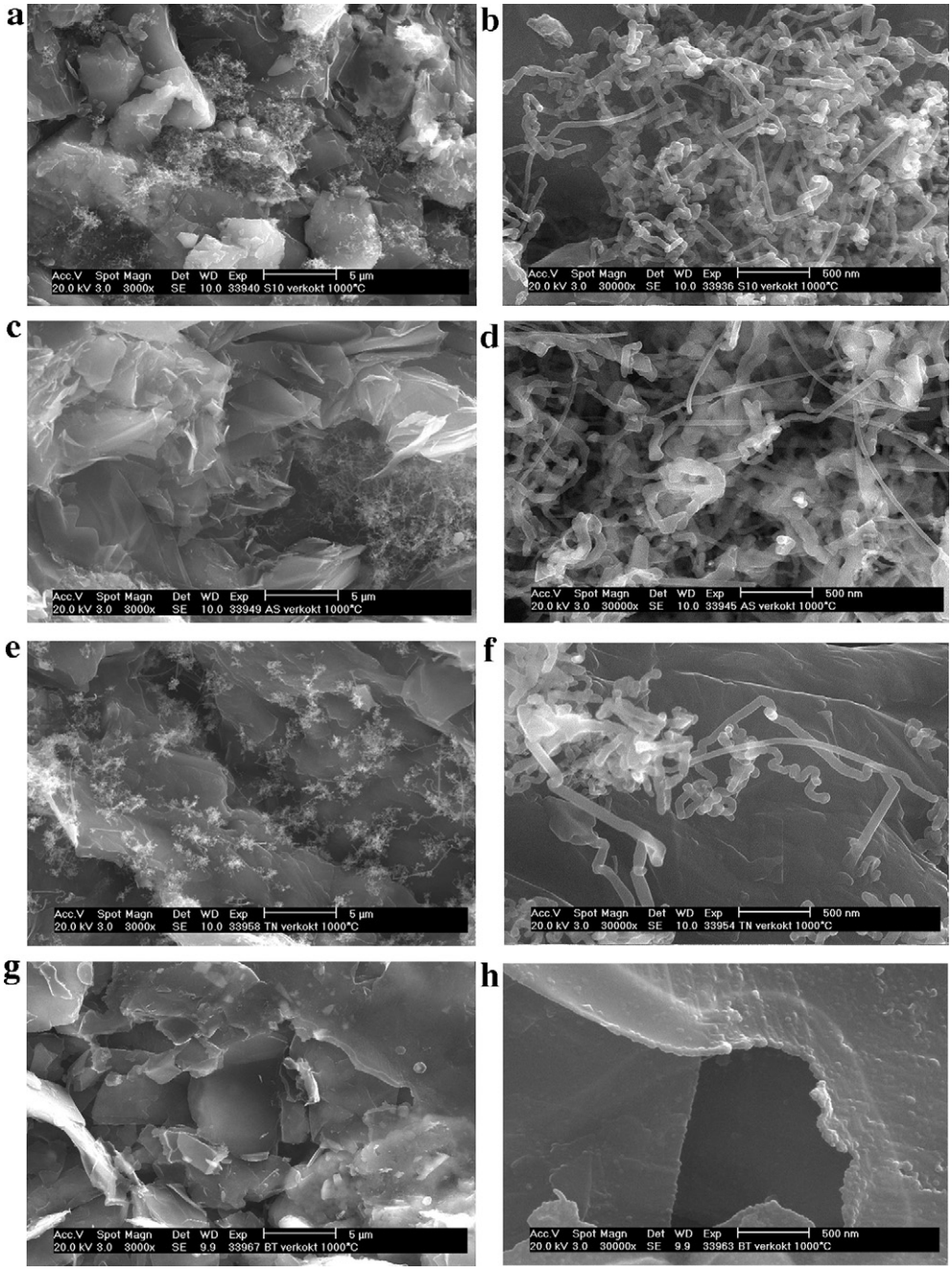

Fig. 3. SEM micrographs of fracture surfaces of the Al_2O_3–C samples with single nanoscaled additives: (a) Spinel (S10), magnification: 3000×; (b) S10, magnification: 30,000×; (c) alumina Sheets (AS), magnification: 3000×; (d) AS, magnification: 30,000×; (e) Chinese CNTs (TN), magnification: 3000×; (f) TN, magnification: 30,000×; (g) German CNTs (BT), magnification: 3000×; (h) BT, magnification: 30,000×.

thermo-mechanical behaviour of the refractory compositions. The composition with the nanoscaled magnesium aluminate spinel addition (S10) showed the best performance, regarding the good CMOR and HMOR values and the lowest strength loss due to thermal shock treatment (11.3%).

3.2. Addition of combinations of nanosized $MgAl_2O_4$, Al_2O_3 and CNTs

The same nanomaterial proportions as in the previous case (single additives) were used for the preparation of the Al_2O_3–C compositions with combinations of nanosized magnesium aluminate spinel with alumina sheets (S10–AS) and carbon nanotubes (S10–TN), as well as carbon nanotubes with alumina sheets (TN–AS), as shown in Table 2.

3.2.1. Influence on the physical properties

The results of the open porosity of the coked samples versus their pore diameter are shown in Fig. 7, whereby the porous structure of the Reference I and the Reference II composition are being presented as well for comparative purposes. A decrease of the pore sizes of the compositions with alumina

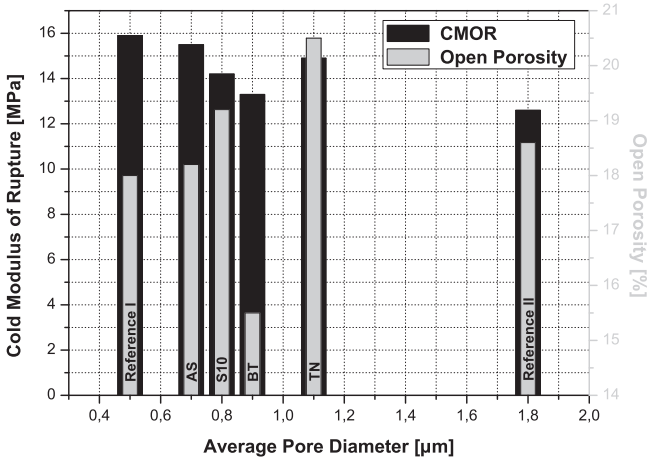

Fig. 4. Cold modulus of rupture, open porosity and average pore diameters of the coked samples with single nanoscaled additives.

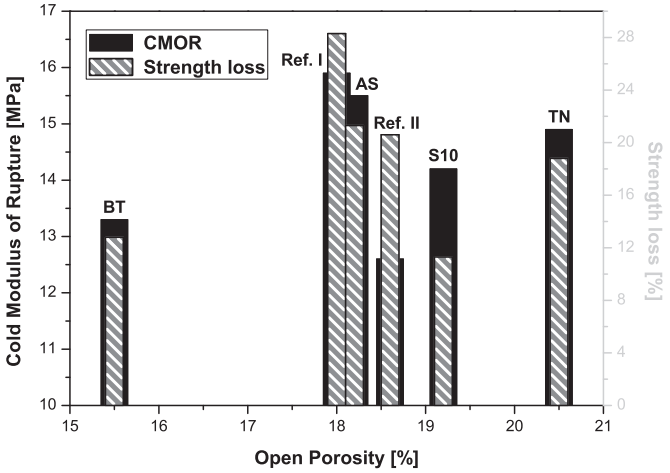

Fig. 6. Cold modulus of rupture and strength loss after 5 thermal shocks versus open porosity of the coked samples with single nanoscaled additives.

nanosheets addition (S10–AS and TN–AS) over the upmost pore diameter range, compared to the Reference II composition, was again evident. This is pointed out in the median pore diameter values of Table 4, with the compositions S10–AS and TN–AS having a mean pore diameter of 1.0 μm and 1.3 μm, respectively. On the other hand, composition S10–TN presented larger pore sizes than the Reference II composition over the upmost pore diameter range, having a mean pore diameter of 2.9 μm (Table 4). The above results come to an agreement with the results of the compositions with nanoscaled materials as single additives, whereby the alumina nanosheets and the magnesium aluminate spinel additives led to a microstructure with much smaller pore sizes than composition TN. However, all three compositions had similar open porosity values (between 18.2% and 18.7%) as shown in Fig. 7 and Table 4. As for the bulk densities, the results come to an agreement with the results of the compositions with single nanomaterial additions: the compositions with magnesium aluminate spinel (S10) and Chinese CNTs (TN) additives presented higher open porosity and lower bulk density values compared to the composition with alumina nanosheets (AS) addition, which exhibited lower open porosity and higher bulk density values.

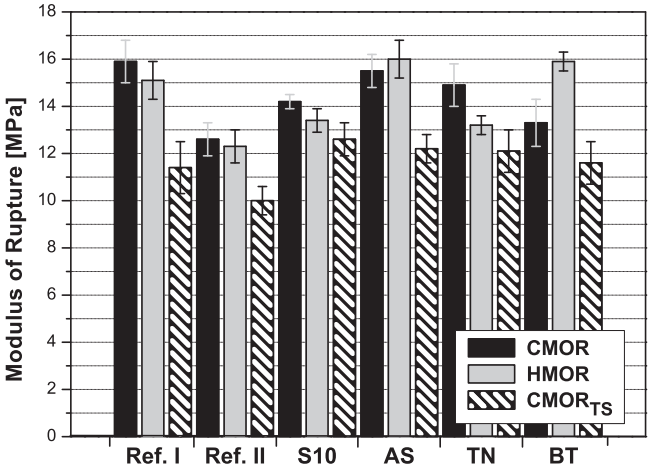

Fig. 5. Cold modulus of rupture (CMOR), hot modulus of rupture (HMOR) and residual $CMOR_{TS}$ after 5 thermal shocks in compressed air of the coked samples with single nanoscaled additives.

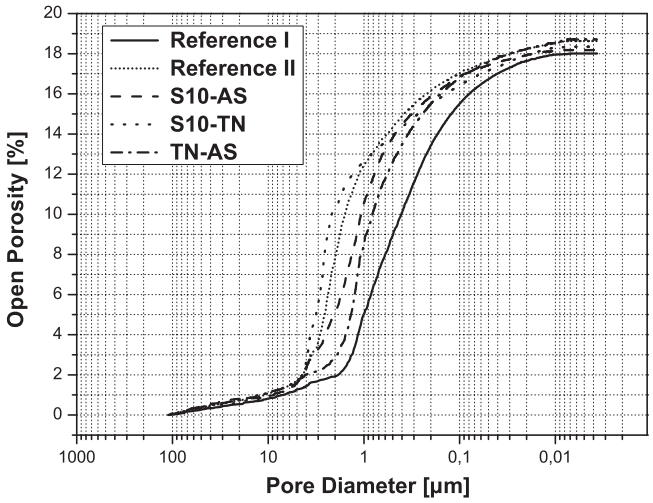

Fig. 7. Open porosity versus pore diameter of the coked samples with combinations of nanoscaled additives.

3.2.2. *Influence on the microstructure*

The microstructure of the Al_2O_3–C refractories with combinations of nanomaterial additions coked at 1.000 °C is shown in Fig. 8. The main characteristic was the unexpected

Table 4
Physical properties of the coked Al_2O_3–C samples with combinations of nanoscaled additives.

Compositions	Physical properties		
	Open porosity (%)	Bulk density (kg/m^3)	Median pore diameter d_{50} (μm)
Reference I	18.0	2.39	0.5
Reference II	18.6	2.51	1.8
S10–AS	18.2	2.50	1.0
S10–TN	18.3	2.46	2.9
TN–AS	18.7	2.51	1.3

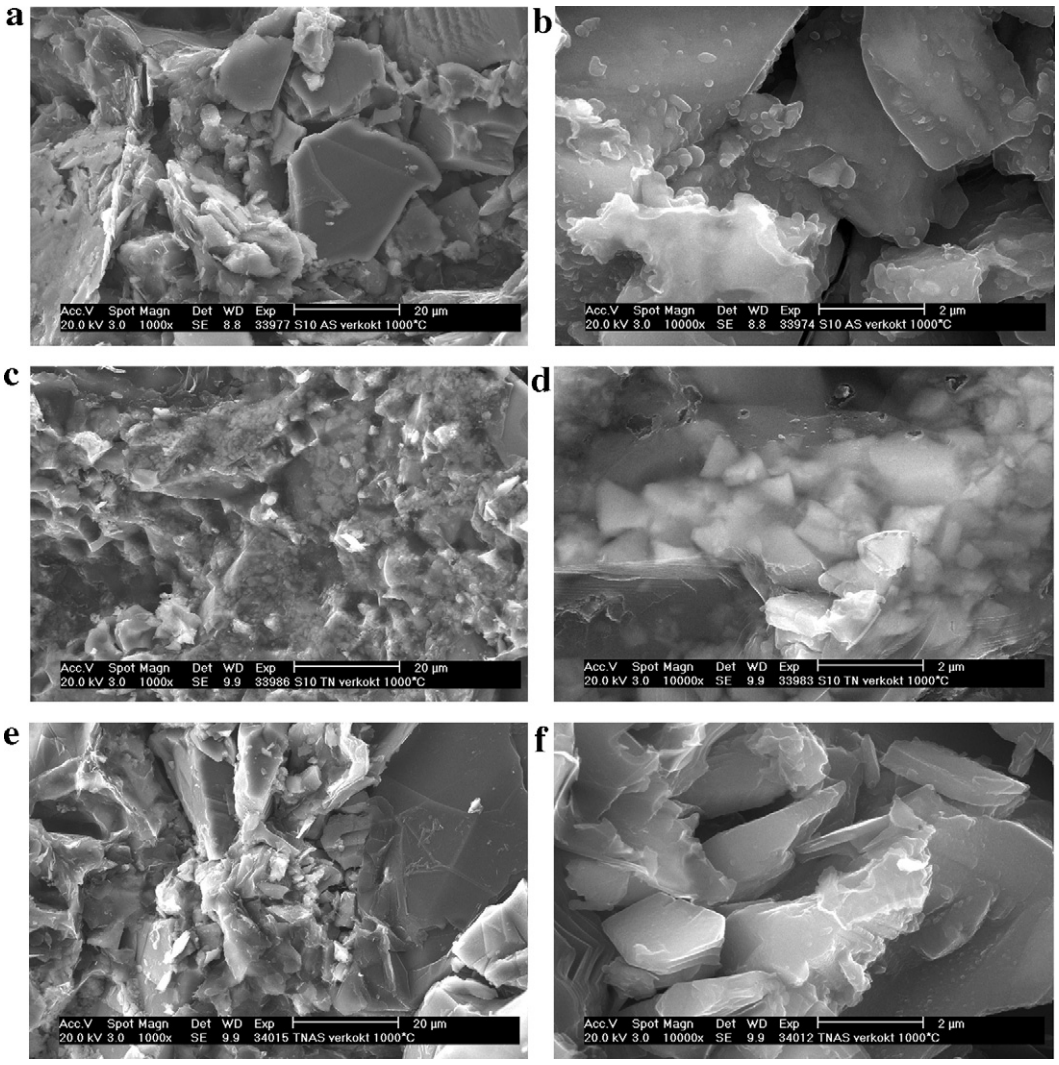

Fig. 8. SEM micrographs of fracture surfaces of the Al_2O_3–C samples with combinations of nanoscaled additives: (a) Spinel and alumina sheets (S10–AS), magnification: 1000×; (b) S10–AS, magnification: 10,000×; (c) Spinel and Chinese CNTs (S10–TN), magnification: 1000×; (d) S10–TN, magnification: 10,000×; (e) Chinese CNTs and Alumina Sheets (TN–AS), magnification: 1000×; (f) TN–AS, magnification: 10,000×.

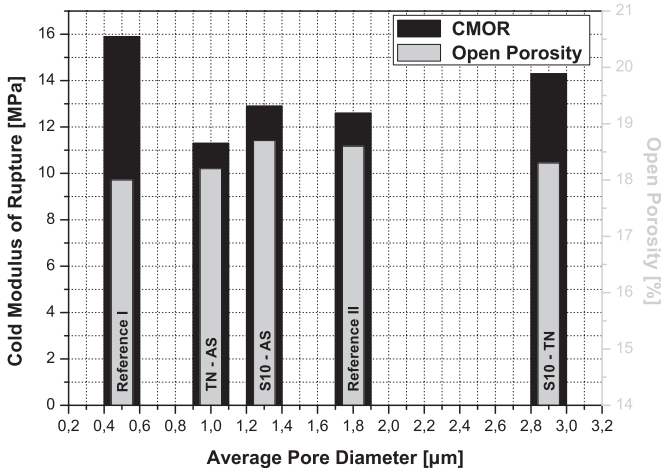

Fig. 9. Cold modulus of rupture, open porosity and average pore diameters of the coked samples with combinations of nanoscaled additives.

absence of in situ formed fibre/whisker structures at all compositions. The reason for this occurrence needs further investigation. The SEM micrographs of fracture surfaces of composition S10–AS in Fig. 8a and b are showing typical microstructural features of Al_2O_3–C refractories, while a homogeneous embedding of the nanoscaled magnesium aluminate spinel crystals in the glassy carbon binder matrix of composition S10–TN is shown in Fig. 8c and d. As for composition TN–AS, the SEM micrographs of fracture surfaces shown in Fig. 8e and f indicate an interlocking network of Al–O-rich (according to the EDS analysis) platelets (Fig. 8f).

3.2.3. Influence on the mechanical and thermo-mechanical properties

Compared to the Reference II composition, the addition of combinations of nanomaterials led to an increase of the CMOR only for composition S10–TN, as shown in Figs. 9 and 10, while composition TN–AS had a comparable CMOR value. This occurrence is attributed to the reinforcement of the binder matrix (Fig. 8d) by the homogeneous distribution of the

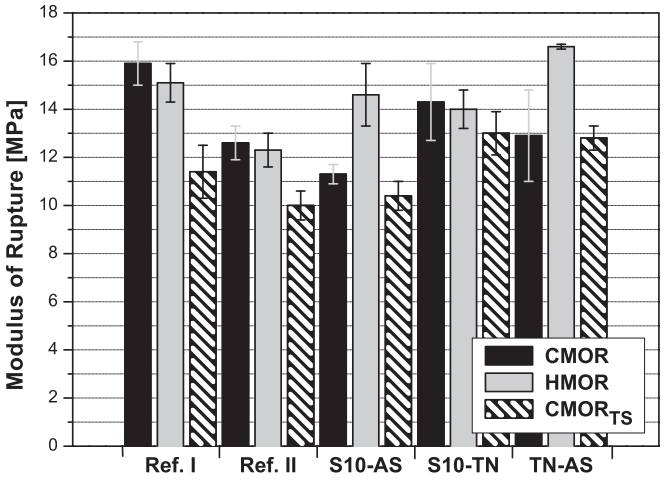

Fig. 10. Cold modulus of rupture (CMOR), hot modulus of rupture (HMOR) and residual $CMOR_{TS}$ after 5 thermal shocks in compressed air of the coked samples with combinations of nanoscaled additives.

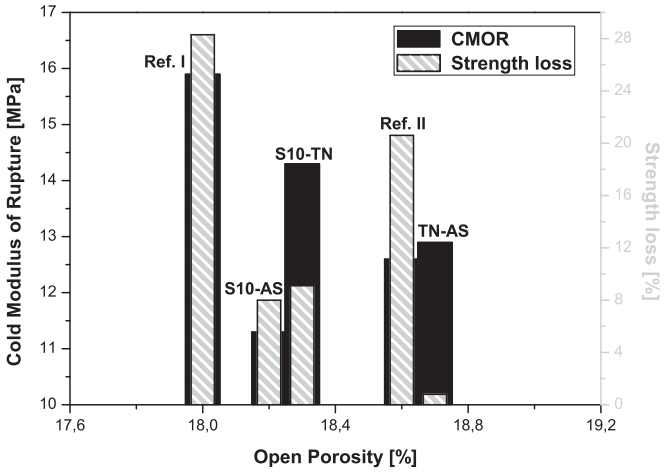

Fig. 11. Cold modulus of rupture and strength loss after 5 thermal shocks versus open porosity of the coked samples with combinations of nanoscaled additives.

Table 5
Summarized properties of the investigated Al_2O_3–C compositions.

Compositions	Properties					
	OP (%)	BD (kg/m^3)	CMOR (MPa)	HMOR (MPa)	$CMOR_{TS}$ (MPa)	Strength loss (5 TS) (%)
Reference I	18.0	2.39	15.9 ± 0.9	15.1 ± 0.8	11.4 ± 1.1	28.3
Reference II	18.6	2.51	12.6 ± 0.7	12.3 ± 0.7	10.0 ± 0.6	20.6
S10	19.2	2.42	14.2 ± 0.3	13.4 ± 0.5	12.6 ± 0.7	11.3
AS	18.2	2.50	15.5 ± 0.7	16.0 ± 0.8	12.2 ± 0.6	21.3
TN	20.5	2.44	14.9 ± 0.9	13.2 ± 0.4	12.1 ± 0.9	18.8
BT	15.5	2.55	13.3 ± 1.0	15.9 ± 0.4	11.6 ± 0.9	12.8
S10–AS	18.2	2.50	11.3 ± 0.4	14.6 ± 1.3	10.4 ± 0.6	8.0
S10–TN	18.3	2.46	14.3 ± 1.6	14.0 ± 0.8	13.0 ± 0.9	9.1
TN–AS	18.7	2.51	12.9 ± 1.9	16.6 ± 0.1	12.8 ± 0.5	0.8

nanoscaled spinel additive. However, the hot modulus of rupture (HMOR) of the coked samples was improved for all compositions and was at comparable levels as in the occasions of single nanoscaled additives (Figs. 5 and 10). As for the thermo-mechanical behaviour of the coked samples, it was improved for all compositions as shown in Fig. 11. The composition with nanoscaled additions of Chinese CNTs and alumina sheets in particular exhibited an outstanding thermal shock resistance, by having a strength loss of only 0.8%. Taking the SEM micrograph in Fig. 8f into account, it can be assumed that the interlocking network of the Al–O-rich platelets contribute to the remarkable thermo-mechanical performance of composition TN–AS. The properties of all investigated compositions are summarized in Table 5.

4. Conclusions

The influence of nanoscaled powders of magnesium aluminate spinel ($MgAl_2O_4$), alumina sheets (α-Al_2O_3) and carbon nanotubes (CNTs) on the microstructure and the physical, mechanical and thermo-mechanical properties of Al_2O_3–C refractories were investigated at the present work. An improvement of the mechanical strength both at room temperature and at 1.400 °C as well as an improvement of the thermal shock resistance of the investigated Al_2O_3–C compositions could be achieved. This was revealed by the microstructural evolution of the refractories after the additions of the nanomaterials by means of the in situ formation of fibres/whiskers after coking at the low temperature of 1.000 °C. The morphology of the in situ formed phases was varying in length, diameter, crystallinity/transparency depending on the nanoscaled materials added, while the addition of nanoscaled magnesium aluminate spinel led to the best results. The addition of nanoscaled alumina sheets led to a higher level of strength values, which in turn had a negative influence on the thermal shock resistance of this composition.

The addition of combinations of nanoscaled additives further improved the properties of the refractories. However, the higher standard deviation values of these compositions (especially compositions S10-TN and TN-AS) imply the difficulty in achieving an optimal homogeneous distribution of the nanomaterials in the refractory matrix. The overall best behaviour regarding the mechanical and thermo-mechanical properties was performed by the composition with nanoscaled additions of Chinese CNTs and alumina sheets.

Acknowledgements

The authors would like to thank the DFG (Deutsche Forschungsgemeinschaft) for funding this work within the Priority Programme 1418. The authors would also like to thank U. Querner for the Hg-porosimetry measurements, A. Friedrich for the XRD-analyses, Dr. B. Ullrich for the SEM-EDS examinations and A. Morgenstern for sample preparation.

References

[1] M.N. Khezrabadi, J. Javadpour, H.R. Rezaie, R. Naghizadeh, The effect of additives on the properties and microstructures of Al_2O_3–C refractories, J. Mater. Sci. 41 (2006) 3027–3032.

[2] A. Yamaguchi, Self-repairing function in the carbon-containing refractory, Int. J. Appl. Ceram. Technol. 4 (6) (2007) 490–495.

[3] H. Sunayama, M. Kawahara, T. Mitsuo, K. Sumitomo, The effect of B_4C addition on the oxidation resistance of Al_2O_3–C and Al_2O_3–SiC–C refractories, in: Proceedings of the Unified International Technical Conference on Refractories, USA, (1997), pp. 841–849.

[4] S. Zhang, A. Yamaguchi, A comparison of Al Si and Al_4SiC_4 added to Al_2O_3–C refractories, in: Proceedings of the Unified International Technical Conference on Refractories, USA, (1997), pp. 861–869.

[5] W. Vieira Jr., B. Rand, The nature of the bond in silicon-containing alumina–carbon refractory composites – Part I, in: Proceedings of the Unified International Technical Conference on Refractories, USA, (1997), pp. 831–840.

[6] S. Zhang, Next generation carbon-containing refractory composites, Adv. Sci. Technol. 45 (2006) 2246–2253.

[7] E. Luhrsen, A. Ott, Immersion nozzles for metal melts, United States Patent 5.171.495, 15. December 1992.

[8] T. Wang, A. Yamaguchi, Antioxidation behavior and effect of $Al_8B_4C_7$ added to carbon-containing refractories, J. Ceram. Soc. Jpn. 108 (9) (2000) 818–822.

[9] M.J. Pitkethly, Nanomaterials – the driving force, Mater. Today 7 (12 Suppl. 1) (2004) 20–29.

[10] S. Tamura, T. Ochiai, S. Takanaga, T. Kanai, H. Nakamura, Nano-Tech. refractories – 1: The development of the nano structural matrix, in: Proceedings of the Unified International Technical Conference on Refractories, Japan, (2003), pp. 517–520.

[11] C.G. Aneziris, D. Borzov, J. Ulbricht, Magnesia-carbon bricks – a high-duty refractory material, Interceram. Refract. Manual (2003) 22–27.

[12] S. Takanaga, T. Ochiai, S. Tamura, T. Kanai, H. Nakamura, Nano-Tech. Refractories – 2: The application of the nano structural matrix to MgO–C bricks, in: Proceedings of the Unified International Technical Conference on Refractories, Japan, (2003), pp. 521–524.

[13] S. Takanaga, Y. Fujiwara, M. Hatta, T. Ochiai, S. Tamura, Nano-Tech. refractories – 3: Development of ''MgO-rimmed MgO–C brick'', in: Proceedings of the Unified International Technical Conference on Refractories, USA, (2005), pp. 148–151.

[14] T. Matsui, K. Goto, Y. Yamada, N. Taki, Characteristics and applications of nano-tech. magnesia carbon bricks, in: Proceedings of the Unified International Technical Conference on Refractories, USA, (2005), pp. 176–179.

[15] Y. Shiratani, T. Yotabun, K. Chihara, T. Ochiai, S. Tamura, Nano-Tech. Refractories – 4: The application of the nano structural matrix to SN plates, in: Proceedings of the Unified International Technical Conference on Refractories, USA, (2005), pp. 575–578.

[16] H. Hattanda, T. Yotabun, T. Tsuda, T. Ochiai, S. Tamura, Nano-Tech. refractories – 7: Application of nano structured matrix to SN plates, in: Proceedings of the Unified International Technical Conference on Refractories, Germany, (2007), pp. 204–207.

[17] K. Haren, K. Morikawa, J. Yoshitomi, K. Asano, Improvement of thermal spalling resistance of alumina–graphite materials by nano-technology, in: Proceedings of the Unified International Technical Conference on Refractories, Germany, (2007), pp. 358–361.

[18] C.G. Aneziris, S.L. Jin, Y.W. Li, V. Roungos, Interactions of carbon nanotubes in Al_2O_3–C refractories for sliding gate applications, in: Summary Booklet (Abstracts) of the Unified International Technical Conference on Refractories, Brazil, (2009), p. 8.

[19] C.G. Aneziris, U. Klippel, W. Schärfl, V. Stein, Y.W. Li, Functional refractory material design for advanced thermal shock performance due to titania additions, Int. J. Appl. Ceram. Technol. 4 (6) (2007) 481–489.

[20] M.A.L. Braulio, M. Rigaud, A. Buhr, C. Parr, V.C. Pandolfelli, Spinel-containing alumina-based refractory castables, Ceram. Int. 37 (2011) 1705–1724.

[21] V.C. Arasu, S. Adak, A.K. Chattopadhyay, C.D. Kamath, Influence of nano-additives on thermo-mechanical properties of alumina castables, in: Summary Booklet (Abstracts) of the Unified International Technical Conference on Refractories, Brazil, (2009), p. 24.

[22] T.R. Lipinski, E. Drygalska, C. Tontrup, The influence of additions of nanostructured Al_2O_3-powder on the high temperature strength of high alumina refractories, in: Summary Booklet (Abstracts) of the Unified International Technical Conference on Refractories, Brazil, (2009), p. 12.

[23] A. Sen, B. Prasad, J.K. Sahu, N. Sahoo, J.N. Tiwari, Effect of nano-oxides and anti-oxidants on corrosion and erosion behavior of submerged nozzle for longer sequence casting of steel, in: Summary Booklet (Abstracts) of the Unified International Technical Conference on Refractories, Brazil, (2009), p. 8.

[24] C.G. Aneziris, J. Hubalkova, R. Barabas, Microstructure evaluation of MgO–C Refractories with TiO_2- and Al- additions, J. Eur. Ceram. Soc. 27 (2007) 73–78.

[25] R.S. Wagner, W.C. Ellis, The vapor–liquid–solid mechanism of crystal growth and its application to silicon, Trans. Met. Soc. AIME 233 (1965) 1053–1064.

[26] G. McMahon, G.J.C. Carpenter, T.F. Malis, On the growth mechanism of silicon carbide whiskers, J. Mater. Sci. 26 (1991) 5655–5663.

[27] P.C. Silva, J.L. Figueiredo, Production of SiC and Si_3N_4 whiskers in C + SiO_2 solid mixtures, Mater. Chem. Phys. 72 (2001) 326–331.

[28] G. Yang, R. Wu, Y. Pan, J. Chen, R. Zhai, L. Wu, J. Lin, Direct observation of the growth process of silicon carbide nanowhiskers by vapor–solid process, Physica E 39 (2007) 171–174.

[29] S. Gustafsson, L.K.L. Falk, E. Liden, E. Carlström, Alumina/silicon carbide composites fabricated via in situ synthesis of nano-sized SiC particles, Ceram. Int. 35 (2009) 1293–1296.

[30] Y.W. Li, C.G. Aneziris, X.X. Yi, S.L. Jin, N. Li, Formation of dumbbell-shaped β-SiC whiskers in Al_2O_3–ZrO_2–C composite refractories, Interceram. Refract. Manual (2005) 20–23.

[31] R. Wu, G. Yang, Y. Pan, J. Chen, R. Zhai, L. Wu, J. Lin, Prism-shaped SiC nanowhiskers, J. Alloys Compd. 453 (2008) 241–246.

[32] L. Guoqi, Y. Bin, L. Hongxia, W. Jinxiang, W. Xinfu, Effect of additives on the properties of Al_2O_3–graphite material heat-treated in nitrogen atmosphere, in: Proceedings of the Unified International Technical Conference on Refractories, Mexico, (2001), pp. 1412–1417.

[33] H. Meyer, H. Hocke, R. Weber, M. Schmid, E. Bramer-Weger, M. Voetz, L. Mleczko, R. Rudolf, A. Wolf, S. Buchholz, Kohlenstoffnanoröhrchenpulver, Kohlenstoffnanoröhrchen und Verfahren zu ihrer Herstellung, German Patent application DE 10 2007 044 031 A1, 19. March 2009.